DOI: 10.1002/ejic.201000632

Synthesis and Characterization of Hierarchically Structured $La_2O_2M@C:Eu^{3+}$ (M = S, Se) Microflowers by a Single-Step RAPET Method

Ramakrishnan Kalai Selvan[a,b] and Aharon Gedanken*[a]

Keywords: Hierarchical structures / RAPET / Lanthanum / X-ray diffraction / HRTEM / UV/Vis spectroscopy

Hierarchically structured $La_2O_2M@C:Eu^{3+}$ (M = S, Se) microflowers have been successfully prepared by a facile one-pot synthesis at a low temperature of 950 °C by the reaction under autogenic pressure at elevated temperature (RAPET) technique. The X-ray diffraction patterns reveal the single-phase formation of hexagonally structured La_2O_2M and $La_2O_2M:Eu^{3+}$ (M = S, Se) microstructures. The optimization of reaction parameters, such as temperature and the molar concentrations of the precursors, for the preparation of monophasic La_2O_2M was evaluated by XRD measurements. Raman spectroscopy measurements allowed for the elucidation of the formation of La_2O_2M (M = S, Se) through examination of the active vibrational modes, and also proved the presence of carbon in the compounds. The field emission scanning electron microscopy (FESEM) and TEM images clearly show the micron-sized rose-like morphology, as well as the nanoflake-like structure of the final products. The high resolution transmission electron microscopy (HRTEM) images reveal well-defined lattice fringes indicating the highly crystalline nature of the products. The selected area electron diffraction (SAED) pattern indicates the single- and polycrystalline nature of the products. The optical properties of the materials have been studied by UV/Vis spectroscopy.

Introduction

Rare earth oxysulfides and -selenides, La_2O_2M (M = S, Se), are technologically important materials because of their promising potential application in various pioneering fields. Because of their unique properties such as high thermal and chemical stability, insolubility in water, high melting point (2000–2200 °C), and luminescent efficiency, they have been used in radiation intensifying screens, fluorescent display tubes, X-ray computed tomography, luminescent biological labels, field emission displays, and as effective catalysts for the reduction of SO_2 by CO.[1–7] Generally, rare earth oxysulfide complexes have C_{3v} point group symmetry, where the rare earth ions are coordinated by four oxygen ions and three sulfur ions in the nearest neighbour positions. The O site symmetry is also C_{3v}, and four rare earth ions are tetrahedrally coordinated to one oxygen ion. The S site is octahedrally coordinated to six rare earths ions and has D_{3d} symmetry.[8]

The synthesis and characterization of different rare earth substituted and unsubstituted lanthanide oxysulfides for various applications have been reported in the literature. Compound La_2O_2S is a wide-band-gap semiconductor with high thermal and chemical stability. Conventionally, La_2O_2S has been prepared at 1100 °C with high-purity La_2O_3 and elemental sulfur as the starting compounds, and with Na_2CO_3 as the flux to enhance product formation.[9] Recently, Jiang et al. prepared La_2O_2S at 300 °C by a two-step gel solvothermal method involving a reaction between an $La(OH)_3$ gel and K_2S.[10] Using a two step boron/sulfur method, Huang et al. prepared one-dimensional La_2O_2S nanostructures under mild conditions.[11] The crystal chemistry, thermal and thermodynamic properties of La_2O_2S have been discussed by Suponitskii et al.[12] Peng et al. have synthesized $La_2O_2S:Eu^{3+}$ by the gel thermolysis method.[13] Using an ethanol-assisted solution combustion method, Luo et al. have prepared an La_2O_2S:Yb,Pr nanometer phosphor at 1000 °C in a reduced atmosphere of 90% N_2 + 10% H_2.[14] Eu^{3+}-substituted La_2O_2S and Eu-, Tb- and Tm-doped Ln_2O_2S (Ln = Y, La, Gd) compounds have been prepared by Xia et al.[15] and Bang et al.[16] by a combustion method with nitrate salts as the starting precursors and highly expensive dithiooxamide as the fuel. Tb^{3+}- and Eu^{3+}-substituted La_2O_2S compounds have been prepared by a coprecipitation method with gelatine as the template and ammonium sulfate as the sulfurizing agent, following a reduction reaction at 750 °C in an H_2 atmosphere.[17] The above-mentioned preparation methods for lanthanide oxysulfides have drawbacks. Some of the methods need reducing atmospheres,[14,17] complicated two-step processes,[10,11] and expensive starting compounds.[15,16] It is very difficult

[a] Department of Chemistry, Kanbar Laboratory for Nanomaterials, Institute of Nanotechnology and Advanced Materials, Bar-Ilan University, Ramat-Gan 52900, Israel
E-mail: gedanken@mail.biu.ac.il
[b] Solid State and Energy Devices Laboratory, Department of Physics, Bharathiar University, Coimbatore 641046, India
E-mail: selvankram@buc.edu.in

Supporting information for this article is available on the WWW under http://dx.doi.org/10.1002/ejic.201000632.

to synthesize La_2O_2M (M = S, Se) by a single-step method. This conclusion led us to develop a new synthetic strategy to prepare this type of technologically important materials in a one-step process conducted at a low reaction temperature. The proposed technique uses easy to handle precursors, simple process control, and is cheap to implement.

Taking into account the above-mentioned criteria, we will present a single-step RAPET method for the synthesis of $La_2O_2M@C:Eu^{3+}$ (M = S, Se). The main advantage of this method is that it is a straightforward single-step process that is solvent-free, catalyst-free, environmentally friendly, and highly reproducible. Using this method, we have previously prepared and reported on the synthesis of various materials such as rare earth hexaboride (RB_6) cubes,[18] WC nanotubes,[19] WS_2 plates,[20] hexagonally shaped SnO_2 nanoparticles,[21] superconducting MgB_2,[22] and a spherical PtP_2/C composite.[23] Herein we report on the synthesis of $La_2O_2M@C:Eu^{3+}$ (M = S, Se) from readily available rare earth metal acetate precursors and elemental S or Se starting compounds. The prepared materials have been characterized by XRD, Raman spectroscopy, FESEM, TEM, HRTEM and UV/Vis measurements. To the best of our knowledge, no single-step syntheses of La_2O_2Se and Eu^{3+}-substituted La_2O_2Se have ever been reported; hence this is the first report of its kind.

Results and Discussion

Structural Properties

The XRD patterns of the prepared $La_2O_2M@C:Eu^{3+}$ (M = S, Se) compounds are shown in Figure 1(a)–(d). All of the XRD patterns show sharp and well-defined peaks, indicating the high crystallinity of the products, and no other secondary phases were observed, which shows the high phase purity of the end products. The observed diffraction peaks appeared at 2θ = 25.34, 28.50, 36.31, 44.61, 46.93, 52.23, 53.87, 59.19, 60.64, 66.84, 71.58, 72.55, 73.29, 77.00° corresponding to diffraction from the following planes: (100), (101), (102), (110), (103), (200), (201), (104), (113), (203), (114), (211), (105) and (212), respectively. The observed 2θ values are consistent with the standard Powder Diffraction File (PDF No. 27 0263) for La_2O_2S. The calculated lattice constant values are given in Table 1 and indicate that the synthesized La_2O_2S belongs to the hexagonal crystal system with the space group $P\bar{3}m1$ (164), and the calculated lattice parameters (a = 4.0625 Å, c = 6.9012 Å) are consistent with the standard PDF values (a = 4.051 Å, c = 6.944 Å). When Eu^{3+} ions are substituted into the La_2O_2S structure, the lattice constants (a = 4.0156 Å, c = 6.8443 Å) decrease. This decrease shows the substitution effect, which follows Vegard's law.[24] The peak positions are also shifted to higher angles. The unit cell volume also decreases, which is due to the difference in the ionic radii of the La^{3+} and Eu^{3+} ions (ionic radii: La^{3+} 1.03 Å, Eu^{3+} 0.94 Å). The calculated X-ray density increases when the structure is doped with Eu^{3+} ions.

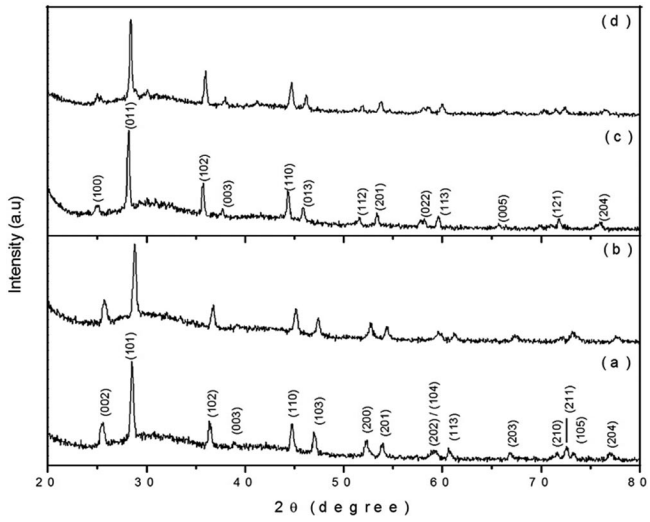

Figure 1. XRD patterns of La_2O_2S (a), $La_2O_2S:Eu^{3+}$ (b), La_2O_2Se (c), and $La_2O_2Se:Eu^{3+}$ (d) microstructures.

The observed diffraction peaks for La_2O_2Se [Figure 1(c),(d)] are well matched with the standard PDF file (PDF No. 74 0346), which suggests the formation of a hexagonal La_2O_2Se structure. The calculated lattice constant values (a = 4.0896 Å, c = 7.1320 Å) are comparable to the standard values (a = 4.07 Å, c = 7.124 Å) for La_2O_2Se. The unit cell parameters decrease (a = 4.0540 Å, c = 7.1043 Å) when Eu^{3+} ions are substituted into the La_2O_2Se structure, due to the difference in ionic radii between the Eu^{3+} and La^{3+} ions. A similar trend was observed for the unit cell volume. No carbon signal was observed for either sample, which may be due to the amorphous or semicrystalline nature of the carbon.

Figure 2 shows the Raman spectra for $La_2O_2M@C:Eu^{3+}$ (M = S, Se) nanostructures measured over the wavenumber range 250–1800 cm^{-1}. The peaks observed in the low wavenumber region, from 250 to 600 cm^{-1}, are assigned to

Table 1. Structural and optical properties of the compounds reported herein.

Compounds	Lattice parameters		Grain size	Quantitative analysis [La/M/Eu (%)][a] Atomic ratio of elements (normalized)				Band gap
	a [Å]	c [Å]	[nm]	Reactants		Products		Eg [eV]
				La/M	Eu/M	La/M	Eu/M	
La_2O_2S	4.0625	6.9012	44	0.4	–	2.23	–	4.12
$La_{1.8}Eu_{0.2}O_2S$	4.0156	6.8443	32	0.36	0.04	1.92	0.21	4.14
La_2O_2Se	4.0896	7.1320	39	0.4	–	1.93	–	4.14
$La_{1.8}Eu_{0.2}O_2Se$	4.0540	7.1043	39	0.36	0.04	1.625	0.175	4.17

[a] M = S, Se.

La_2O_2M (M = S, Se). According to factor group analysis,[8] the α-phase of La_2O_2S has the following lattice vibrations: $\Gamma = 2A_{1g} + 3A_{2u} + 2E_g + 3E_u$, where the four g modes are Raman-active, and four of the u modes are IR-active. The remaining two u modes are acoustic. The two strong peaks observed at 361.0 and 391.4 cm^{-1} in the Raman spectra of the La_2O_2S products are assigned to Raman-active modes E_g and A_{1g}, respectively. These Raman bands are in good agreement with earlier reported spectra (360 and 392 cm^{-1}).[25] On the other hand, the spectrum for La_2O_2Se shows one sharp high-intensity peak at 393 cm^{-1} within the measured frequency range corresponding to the Raman-active mode A_{1g}. It can be concluded that the Raman spectra also substantiate the assignment of the products as La_2O_2M (M = S, Se).

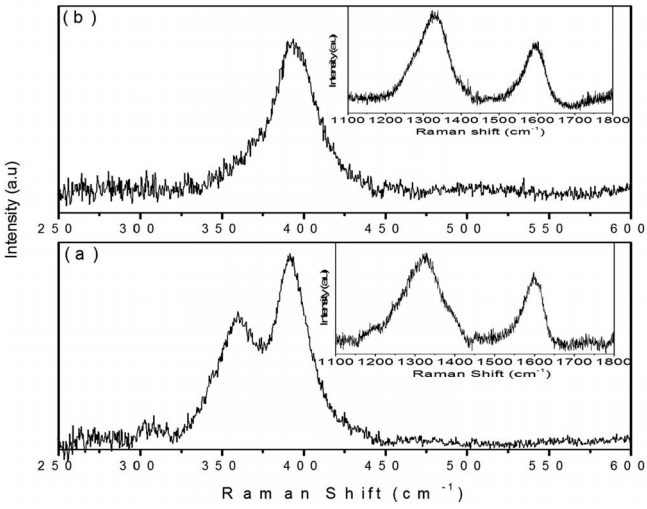

Figure 2. Raman spectra of La_2O_2S@C (a) and La_2O_2Se@C (b) microstructures.

In order to identify the presence of carbon in the La_2O_2M (M = S, Se) samples, the Raman spectra were also measured in the wavenumber region 1000–1800 cm^{-1} (inset of Figure 2). Characteristic carbon peaks were observed at 1327 and 1600 cm^{-1} in the spectrum of La_2O_2S, and at 1330 and 1593 cm^{-1} in the spectrum for the La_2O_2Se particles, which indicates the presence of carbon in the prepared samples. The band at around 1350 cm^{-1} is assigned to disordered carbon (D), which corroborates the occurrence of defects in the hexagonal graphitic layers. Similarly, the band at around 1590 cm^{-1} represents graphitic carbon (G), and corresponds to an E_{2g} mode of graphite, which is due to the sp^2-bonded carbon atoms in a two-dimensional hexagonal graphitic layer.[26] The intensity ratios (I_D/I_G) of the graphitic D and G bands are 1.205 and 1.197 for La_2O_2S and La_2O_2Se, respectively, which indicates that the materials contain disordered amorphous carbon with a high content of lattice defects.[27] The percentage of carbon, according to the C,H,N analyses, in the prepared samples is 4.066, 5.067, 4.276 and 1.256 for La_2O_2S, La_2O_2S:Eu^{3+}, La_2O_2Se and La_2O_2Se:Eu^{3+}, respectively.

Morphological Properties

In order to analyze the morphological features of the materials, FESEM analyses were carried out for all samples. Figure 3 shows the FESEM image of hierarchically structured La_2O_2S (a, b) and La_2O_2S:Eu^{3+} (c, d) at two different magnifications. At low magnification, the image of La_2O_2S reveals the formation of a rose-like hierarchical structure of 12–14 μm in size. The magnified image shows that the rose-like morphology is constructed from small plate-like particles with an average size of 2–3 μm, and some spherical particles. However, the plate-like structure is not clear in the low magnification images. On the other hand, La_2O_2S:Eu^{3+} [Figure 3(c),(d)] demonstrates an entirely different morphology. This compound is built of nest-like structures in addition to various rose-like microstructures. A close examination of the La_2O_2S:Eu^{3+} images provides an explanation for the formation of the hierarchical structure that is assembled from several 2D sheets through an oriented self-assembly arrangement. It can also be seen that the individual sheets are closely packed in order to maintain their integrity, and as such they form the hierarchical structure. The thickness of the plates is nearly 10 nm, and the diameter of the plates is in the micrometer range. Energy dispersive spectroscopy (EDAX) [Supporting Information, Figure S1(a),(b)] results demonstrate the presence of the constituent elements, such as La, O and S, of La_2O_2S, as well as La, O, S and Eu in the La_2O_2S:Eu^{3+} sample. Quantitative analysis results (Table 1) show that the atomic ratio of La/S is about 2.23 for La_2O_2S, which indicates that this compound is S-deficient. This may be due to the volatile nature of sulfur compounds at high temperatures. However, XRD data and Raman spectra confirm the phase of the

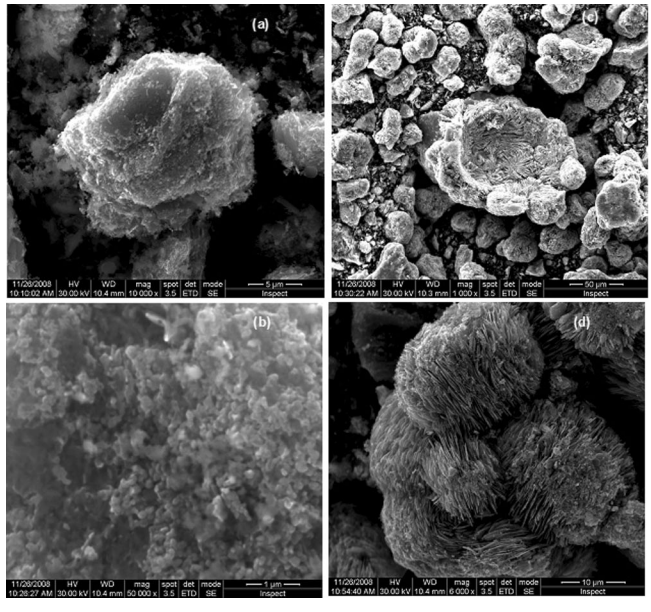

Figure 3. FESEM images of La_2O_2S (a, b) and La_2O_2S:Eu^{3+} (c, d); [scale bar: 5 μm (a), 1 μm (b), 50 μm (c) and 10 μm (d)].

La_2O_2S structure. Figure 4 shows the selected area of the elemental X-ray dot mapping of $La_2O_2S:Eu^{3+}$, which displays the distribution of the La, Eu, S, O and C elements in the sample. The images show that all the elements are uniformly distributed over the scanned area. There is no distinct area of the sample that gives rise to the Eu signals, which indirectly reveals the single-phase formation of the Eu^{3+}-doped La_2O_2S. Similar observations were made for the FESEM images of La_2O_2Se and $La_2O_2Se:Eu^{3+}$, which are illustrated in Figure 5. The magnified image of La_2O_2Se [Figure 5(a)] reveals that the prepared material exhibits hierarchical rose-like structures that have an average size of around 40 μm. Close examination of a single rose shows that plate-like particles are arranged by self-assembly to form the individual roses. The corresponding EDAX [Supporting Information, Figure S2(a)] pattern is attributed to the elements that are presented in the sample. The calculated atomic ratio of La/Se is 1.93, which is very close to the stoichiometric ratio in the compound formula, La_2O_2Se. The FESEM image of Eu^{3+}-doped La_2O_2Se is given in Figure 5(b). The image is similar to those of the doped sulfide, but with microstructures of different sizes. At close observation, the image shows the hierarchical rose-like morphology of the sample. The EDAX pattern confirms the presence of La, Eu, O and Se elements [Supporting Information, Figure S2(b)]. Figure 6 shows the selected area for elemental electron dot mapping of $La_2O_2Se:Eu^{3+}$. It can be seen that C is present over the whole surface of the individual roses, and the La, Eu, Se and O pattern suggests a uniform distribution of these elements in the sample. No separate signals are observed for any of the individual elements.

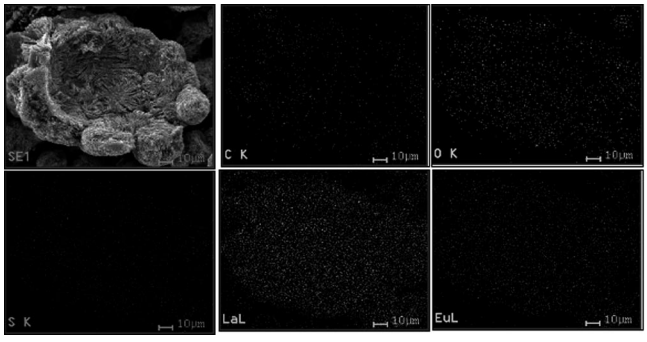

Figure 4. X-ray elemental electron mapping images of $La_2O_2S:Eu^{3+}$ (scale bar: 10 μm for all images).

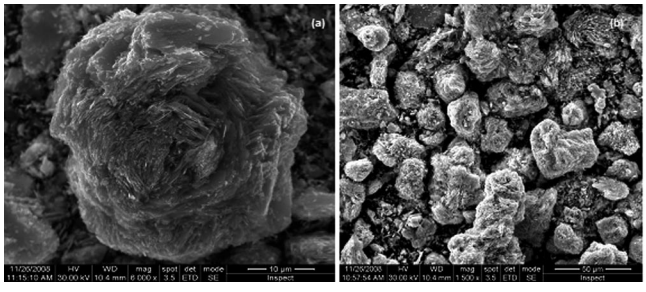

Figure 5. FESEM images of La_2O_2Se (a) and $La_2O_2S:Eu^{3+}$ (b) [scale bar: 10 μm (a) and 50 μm (b)].

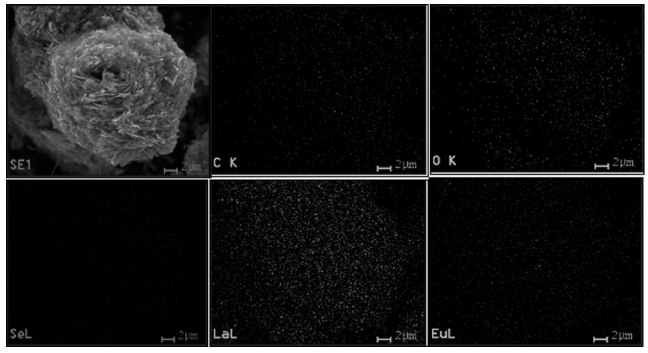

Figure 6. Electron mapping images of $La_2O_2Se:Eu^{3+}$ (scale bar: 2 μm for all images).

The TEM images and SAED patterns of pristine- and Eu^{3+}-substituted La_2O_2S and La_2O_2Se are given in Figure 7. At high magnification, triangle-shaped plate-like structures are observed instead of rose- or nest-like hierarchical structures. This may be due to the ultrasonication treatment of the final products; the flowers are aggregates of individual nanoparticles.[28] Individual particles of La_2O_2S [Figure 7(a)] and $La_2O_2S:Eu^{3+}$ [Figure 7(b)] appear as flakes/plates that are 2–5 μm in size. A ring pattern is observed in the SAED data, which indicates the polycrystalline nature of the materials [Figure 7(c)].

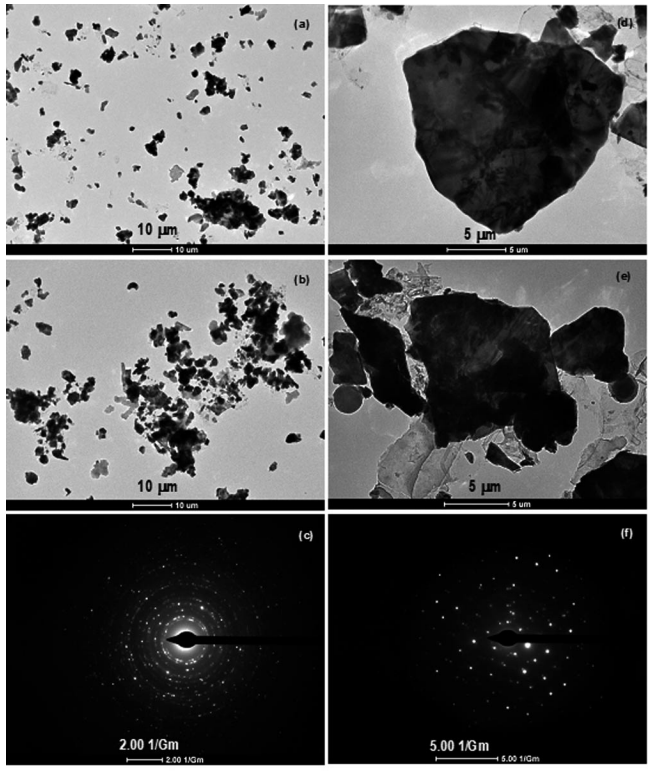

Figure 7. TEM images of La_2O_2S (a), $La_2O_2S:Eu^{3+}$ (b) La_2O_2Se (c), and $La_2O_2Se:Eu^{3+}$ (d). SAED patterns of $La_2O_2S:Eu^{3+}$ (e) and $La_2O_2Se:Eu^{3+}$ (f).

The TEM images of La_2O_2Se and $La_2O_2Se:Eu^{3+}$ [Figure 7(d),(e)] show the individual particles that are more than 10 μm in size and are triangular in shape. The corre-

sponding SAED patterns [Figure 7(f)] show dot patterns that indicate the single-crystalline nature of the materials. In order to further confirm the crystallinity and phase formation, the materials were subjected to HRTEM analysis. The HRTEM images of La_2O_2S and La_2O_2Se are given in Figure 8. At high magnification, both the samples show well-defined lattice fringes, which is attributed to the high crystallinity of the end products. The measured inter-plane spacings, "*d*", are 3.1419 and 3.5478 Å for the (101) and (100) planes of La_2O_2S and La_2O_2Se, respectively. These results further confirm the single-phase formation of the La_2O_2S and La_2O_2Se microstructures. The measured "*d*" values are in good agreement with those reported in the corresponding PDFs (PDF No. 27 0263 for La_2O_2S and 74 0346 for La_2O_2Se). Moreover, the HRTEM image (Supporting Information, Figure S3) shows that the flowers comprise small nanoparticles that are 100–200 nm in size.

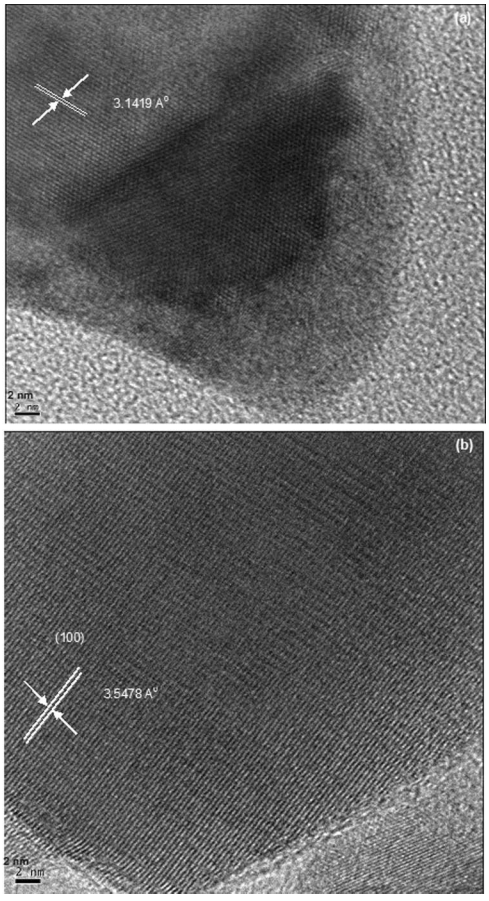

Figure 8. HRTEM images of La_2O_2S (a) and La_2O_2Se (b).

Optical Properties

UV/Vis diffused reflectance spectroscopy (DRS) measurements were carried out to calculate the optical band-gap values (*Eg*) (Table 1) for the synthesized materials, and the spectra are depicted in Figure S4 (Supporting Information). The spectra reflect the structural variation of the products that is also manifest in the band-gap values, which are calculated from the relation $Eg = 1240/\lambda$, where λ is the wavelength of the fundamental absorption edge in nanometers. The absorption edge was defined as the wavelength at the intersection obtained by extrapolating the horizontal and sharply rising portions of the UV/Vis absorption curve. The calculated band-gap values are 4.12, 4.14, 4.14 and 4.17 eV for La_2O_2S, $La_2O_2S:Eu^{3+}$, La_2O_2Se and $La_2O_2Se:Eu^{3+}$, respectively. Unfortunately, Eu^{3+} doping of the parent structures has no significant influence on the band-gap values. Similar band-gap values were calculated for Sm_2O_2S (4.2 eV) and Eu_2O_2S (4.4 eV) nanostructures.[29]

Reaction Mechanism

A few control experiments have been performed to optimize the single-phase formation of La_2O_2M (M = S, Se). For the synthesis of La_2O_2Se, we used the exact stoichiometry [0.003 mol of $La(CH_3COO)_3$ and 0.0015 mol of Se] of starting compounds. XRD analysis confirmed that the product contained an La_2O_3 impurity, which highlighted the Se deficiency of the product. Hence, we repeated the reaction with different concentrations of excess Se (0.0015, 0.0045, 0.0075, 0.0105 and 0.015 mol). Based on the XRD analysis, the appropriate excess for the synthesis of single-phase La_2O_2Se is 0.0075 mol. Furthermore, to optimize the operating temperature, the experiments (with a fivefold excess of Se) were carried out at different temperatures of 800, 850, 900 and 950 °C for 10 h. Finally, at 950 °C we obtained single-phase La_2O_2Se microstructures. The suggested reaction mechanism for the synthesis of La_2O_2Se is as follows:[18,30–32]

$2\ La(CH_3COO)_3{\cdot}xH_2O \rightarrow 2\ La(CH_3COO)_3 + x\ H_2O$

$2\ La(CH_3COO)_3 \rightarrow La_2O(CO_3)_2 + 3\ CH_3COCH_3 + CO_2$

$La_2O(CO_3)_2 \rightarrow La_2O_3 + 2\ CO_2$

$CH_3COCH_3 \rightarrow CO + C_2H_6$

$2\ CO \rightarrow C + CO_2$ (Boudouard reaction)

$2\ La_2O_3 + 2\ Se \rightarrow 2\ La_2O_2Se + O_2$

Conclusions

We have reported on the facile single-step synthesis of hierarchically structured $La_2O_2M:Eu^{3+}$ (M = S, Se) compounds from easily available starting precursors by the RAPET method. The XRD data and Raman spectra confirmed the single-phase formation of the end products. The Raman spectra also confirm the presence of carbon in the products, which comes from the decomposition of the acetate precursors. The formation of hierarchical structures with rose- and nest-like morphologies was apparent from the FESEM images of the materials. The selected area electron mapping images and EDAX patterns confirm the uniform distribution of Eu in the doped La_2O_2M (M = S, Se) compounds. The high crystallinity of the materials was confirmed by HRTEM analysis.

Experimental Section

$La(CH_3COO)_3{\cdot}xH_2O$, $Eu(CH_3COO)_3{\cdot}xH_2O$, and elemental S or Se (Aldrich) were starting compounds. The reaction was carried out in a 5 mL stainless steel Swagelok closed cell. A 1/2″ union part was plugged on both sides by standard caps, as described elsewhere.[18–23] For the typical synthesis of La_2O_2Se, anhydrous $La(CH_3COO)_3$ (0.003 mol, 0.9482 g) and an excess of Se (0.0075 mol, 0.5918 g) were introduced into the cell at room temp. under nitrogen. The amount of Eu doping was 0.0003 mol. The filled cell was tightly closed with another plug, and then placed inside an iron pipe in the middle of a furnace. The temperature was raised to 950 °C at a heating rate of 10 °C/min and maintained at 950 °C for 10 h. The reaction proceeded under the autogenic pressure of the precursors. The Swagelok cell was then gradually cooled to room temp. (over 5 h), opened with the release of a little pressure, and the resultant final product collected without any further processing. The yield of the final products was 58, 62, 55 and 60% for La_2O_2S@C, La_2O_2S@C:Eu^{3+}, La_2O_2Se@C and La_2O_2Se@C:Eu^{3+}, respectively. A similar procedure was adopted for the synthesis of the rest of the compounds reported herein. The X-ray diffraction patterns of the products were measured with a Bruker AXS D* Advance Powder X-ray diffractometer (Cu-K_α: λ = 1.5418 Å). The particle morphology and structures were studied by TEM (JEOL-JEM 100 SX TEM microscope) with an accelerating voltage of 80 kV, and a JEOL-2010 HRTEM with an accelerating voltage of 200 kV. HRSEM measurements of the products were carried out with a JEOL-JSM 840 operating at 10 kV. Raman spectra for the materials were recorded with a Jobin Yvon Horiba Raman System. The 632.8 nm line of a He-Ne laser was the excitation source (40% power) focused to a 1–2 μm spot size. The UV/Vis DRS data were recorded with a Perkin–Elmer UV/Vis spectrophotometer. Before measuring the optical properties, the samples were calcined at 600 °C in air atmosphere for 3 h to remove the carbon.

Supporting Information (see footnote on the first page of this article): EDX patterns of La_2O_2S, La_2O_2S:Eu^{3+}, La_2O_2Se and La_2O_2Se:Eu^{3+}, HRTEM image of La_2O_2S and La_2O_2Se microstructures and UV/Vis spectra of La_2O_2M:Eu^{3+} (M = S and Se) compounds.

[1] J. X. Ma, M. Fang, W. T. Lau, *J. Catal.* **1996**, *158*, 251–259.
[2] R. V. Alves, R. A. Buchanan, K. A. Wickersheim, E. A. C. Yates, *J. Appl. Phys.* **1971**, *42*, 3043–3048.
[3] L. Ozawa, *J. Electrochem. Soc.* **1977**, *124*, 413–417.
[4] G. F. J. Garlick, C. L. Richards, *J. Lumin.* **1974**, *9*, 432–439.
[5] J. Ma, M. Fang, N. T. Lau, *Appl. Catal. A* **1997**, *150*, 253–268.
[6] S. Cho, J. Yoo, J. Lee, *J. Electrochem. Soc.* **1998**, *145*, 1017–1019.
[7] H. Yamamoto, T. Kana, *J. Electrochem. Soc.* **1979**, *126*, 305–312.
[8] S. Yokono, S. Imanaga, T. Hoshina, *J. Phys. Soc. Jpn.* **1979**, *46*, 1882–1888.
[9] M. R. Rayce, A. L. Smith, P. N. Yocon, U. S. Patent 3,413,246, **1968**.
[10] Y. Jiang, Y. Wu, Y. T. Qian, *J. Am. Ceram. Soc.* **2000**, *83*, 2628–2630.
[11] Y. Z. Huang, L. Chen, L. M. Wu, *Cryst. Growth Des.* **2008**, *8*, 739–743.
[12] Y. L. Suponitskii, G. M. Kuz′micheva, A. A. Eliseev, *Russ. Chem. Rev.* **1988**, *57*, 209–220.
[13] H. Peng, S. Huang, F. You, J. Chang, S. Lu, L. Cao, *J. Phys. Chem. B* **2005**, *109*, 5774–5778.
[14] X. Luo, W. H. Cao, *J. Alloys Compd.* **2008**, *460*, 529–534.
[15] T. Xia, W. H. Cao, Y. Tian, *J. Mater. Res.* **2005**, *20*, 2274–2278.
[16] J. Bang, M. Abboudi, B. Abrams, P. H. Holloway, *J. Lumin.* **2004**, *106*, 177–185.
[17] Z. Liu, X. Sun, S. Xu, J. Lian, X. Li, Z. Xiu, Q. Li, D. Huo, J. G. Li, *J. Phys. Chem. C* **2008**, *112*, 2353–2358.
[18] R. K. Selvan, I. Genish, I. Perelshtein, J. M. C. Moreno, A. Gedanken, *J. Phys. Chem. C* **2008**, *112*, 1795–1802.
[19] S. V. Pol, V. G. Pol, A. Gedanken, *Adv. Mater.* **2006**, *18*, 2023–2027.
[20] V. G. Pol, S. V. Pol, N. Perkas, A. Gedanken, *J. Phys. Chem. C* **2007**, *111*, 134–140.
[21] R. Kalai Selvan, I. Perelshtein, N. Perkas, A. Gedanken, *J. Phys. Chem. C* **2008**, *112*, 1825–1830.
[22] V. G. Pol, S. V. Pol, I. Felner, A. Gedanken, *Chem. Phys. Lett.* **2006**, *433*, 115–119.
[23] P. P. George, A. Gedanken, A. Gabashvili, *Mater. Res. Bull.* **2007**, *42*, 626–632.
[24] R. Kalai Selvan, A. Gedanken, *Nanotechnology* **2009**, *20*, 105602.
[25] C. R. Gopinath, I. D. Brown, *J. Raman Spectrosc.* **1982**, *12*, 278–280.
[26] S. Shanmugam, A. Gedanken, *Electrochem. Commun.* **2006**, *8*, 1099–1105.
[27] V. G. Pol, S. V. Pol, J. M. C. Moreno, A. Gedanken, *Carbon* **2006**, *44*, 3285–3292.
[28] J. Xia, H. Li, Z. Luo, K. Wang, S. Yin, Y. Yan, *Appl. Surf. Sci.* **2010**, *256*, 1871–1877.
[29] J. Llanos, V. Sanchez, C. Mujica, A. Buljan, *Mater. Res. Bull.* **2002**, *37*, 2285–2291.
[30] S. Bhattacharyya, I. Perelshtein, O. Moshe, D. H. Rich, A. Gedanken, *Adv. Funct. Mater.* **2008**, *18*, 1641–1653.
[31] S. Bhattacharyya, D. Zitoun, Y. Estrin, O. Moshe, D. H. Rich, A. Gedanken, *Chem. Mater.* **2009**, *21*, 326–335.
[32] S. V. Pol, V. G. Pol, I. Felner, A. Gedanken, *Eur. J. Inorg. Chem.* **2007**, *14*, 2089–2096.

Received: June 6, 2010
Published Online: November 12, 2010

